processes

MDPI

Article

Preparation of Heat and Salt Resistant Foam Composite System Based on Weathered Coal Particle Strengthening and a Study on Foam Stabilization Mechanism

Yanyan Xu [1,2], Linghui Xi [1,2], Yajun Wu [1,2], Xin Shi [1,2], Zhi Kang [1,2], Beibei Wu [1,2] and Chao Zhang [3,4,*]

[1] Sinopec Northwest Company of China Petroleum and Chemical Corporation, Urumqi 830011, China; xuyany.xbsj@sinopec.com (Y.X.); xilh56632.xbsj@sinopec.com (L.X.); wuyaj.xbsj@sinopec.com (Y.W.); shixin.xbsj@sinopec.com (X.S.); kangzh1115.xbsj@sinopec.com (Z.K.); wubb1474.xbsj@sinopec.com (B.W.)
[2] Sinopec Key Laboratory of Enhanced Oil Recovery for Fractured Vuggy Reservoirs, Urumqi 830011, China
[3] Key Laboratory of Unconventional Oil & Gas Development (China University of Petroleum (East China)), Ministry of Education, Qingdao 266580, China
[4] School of Petroleum Engineering, China University of Petroleum (East China), Qingdao 266580, China
* Correspondence: zhangc@upc.edu.cn

Abstract: Nitrogen foam is a promising enhanced oil recovery (EOR) technique with significant potential for tertiary oil recovery. This improves the efficiency of the oil displacement during the gas drive processes while expanding the swept volume. However, in the high-temperature, high-salinity reservoirs of the Tahe Oilfield, conventional N_2 foam systems show suboptimal performance, as their effectiveness is heavily limited by temperature and salinity. Consequently, enhancing the foam stability under these harsh conditions is crucial for unlocking new opportunities for the development of Tahe fracture-vuggy reservoirs. In this study, the Waring–Blender method was used to prepare weathered coal particles as a foam stabilizer. Compared to conventional foam stabilizers, weathered coal particles were found to enhance the stability of the liquid film under high-temperature and high-salinity conditions. Firstly, the foaming properties of the six foaming agents were comprehensively evaluated and their foaming properties were observed at different concentrations. YL-3J with a mass concentration of 0.7% was selected. The foaming stabilization performance of four types of solid particles was evaluated and weathered coal solid particles with a mass concentration of 15% and particle size of 300 mesh were selected. Therefore, the particle-reinforced foam system was determined to consist of "foaming agent YL-3J (0.7%) + weathered coal (15.0%) + nitrogen". This system exhibited a foaming volume of 310 mL at 150 °C and salinity of 210,000 mg/L, with a half-life of 1920 s. Finally, through interfacial tension and viscoelastic modulus tests, the synergistic mechanism between weathered coal particles and surfactants was demonstrated. The incorporation of weathered coal particles reduced the interfacial tension of the system. The formation of a skeleton at the foam interface increased the apparent viscosity and viscoelastic modulus, reduced the liquid drainage rate from the foam, and mitigated the disproportionation effect. These effects enhanced the temperature, salinity resistance, and stability of the foam. Consequently, they contributed to the stable flow of foam under high-temperature and high-salinity conditions in the reservoir, thereby improving the oil displacement efficiency of the system.

Keywords: N_2 foam; weathered coal particles; foaming volume; half-life; foam stabilization mechanism

check for updates

Academic Editor: Paolo Trucillo

Received: 29 November 2024
Revised: 30 December 2024
Accepted: 6 January 2025
Published: 10 January 2025

Citation: Xu, Y.; Xi, L.; Wu, Y.; Shi, X.; Kang, Z.; Wu, B.; Zhang, C. Preparation of Heat and Salt Resistant Foam Composite System Based on Weathered Coal Particle Strengthening and a Study on Foam Stabilization Mechanism. *Processes* **2025**, *13*, 183. https://doi.org/10.3390/pr13010183

Copyright: © 2025 by the authors. Licensee MDPI, Basel, Switzerland. This article is an open access article distributed under the terms and conditions of the Creative Commons Attribution (CC BY) license (https://creativecommons.org/licenses/by/4.0/).

1. Introduction

The fracture-vuggy reservoir space in the Tahe Oilfield displays a heterogeneous nature with complex structures and highly variable reservoir properties. During the development process, the formation energy diminishes, leading to substantial accumulation of the remaining oil in the upper portion of the reservoir as a result of the density differences between oil and water in the later stages of waterflood development [1–3]. Numerous studies have investigated the feasibility of nitrogen flooding in fracture-vuggy carbonate reservoirs and concluded that this technique has significant potential for enhancing oil recovery, particularly through the artificial gas cap displacement of attic oil [4]. However, field tests have revealed several challenges, such as gas channeling along dominant pathways, pronounced gravity segregation effects, and a high gas-liquid mobility ratio [5–8]. These factors lead to an increase in inefficient and ineffective gas channeling in wells or well groups over time, resulting in reduced efficiency of nitrogen injection for enhanced oil recovery [9,10].

Practical experience has shown that nitrogen foam can seal high-permeability layers, control channeling, adjust the water intake profile, reduce crude oil viscosity, and improve its rheology. Notably, its positive effect on enhancing the gas drive makes it an effective method for nitrogen injection to improve the oil recovery in fracture-vuggy carbonate reservoirs [11–13]. Currently, 10–20 wells in the Tahe Oilfield are treated annually using this technology, although they are still in the developmental stage. Two foam systems have been developed for the harsh conditions of high temperature, pressure, and salinity in the Tahe Oilfield: a compound foam system and a gel-gel foam system [14–18]. However, owing to severe formation conditions, the compound foam system has a half-life of only 7 min, with a defoaming half-life of 20 min, resulting in poor stability. The gel-foam system exhibits only 65% foaming performance, is brittle under shear, and has low toughness. Therefore, the development of a high-stability foam system is urgently needed to further enhance the efficiency of foam flooding [18–22].

To address these challenges, this study proposes the development of a particle-reinforced viscoelastic gas-displacement foam system tailored for fracture-vuggy reservoirs. The aim is to construct a novel foam with enhanced stability and temperature resistance, improve its ability to prevent nitrogen gas channeling in fracture-vuggy formations, increase the nitrogen swept volume, and ultimately improve the nitrogen displacement efficiency. The technical advancements discussed in this paper can provide valuable guidance for the efficient development of nitrogen injection in the fracture-vuggy reservoirs of the Tahe Oilfield.

2. Experimental Section

2.1. Materials

The gas used in the experiment was nitrogen (N_2) with a purity of 99.9 mol% supplied by Qingdao Tianyuan Gas Co., Ltd. (Qingdao, China). The relevant parameters of the formation water used in this experiment are listed in Table 1. Four types of particles were utilized as additives for foaming agents in the experiment: fly ash (CF), weathered coal (RC), CIK (1000 mesh graphite), and graphite milk (LC). The solid particles used in this experiment were supplied by the Northwest Oilfield Branch of China Petrochemical Co. Ltd. (Urumqi, China). The relevant surfactant parameters are presented in Table 2.

Table 1. Preparation of inorganic salts in mineralized formation water.

Mineralization Ratio/($\times 10^4$ mg·L^{-1})	NaCl/(g·L^{-1})	$CaCl_2$/(g·L^{-1})	$MgCl_2$/(g·L^{-1})	Na_2SO_4(g·L^{-1})
21	182.23	31.281	4.6	0.234

Table 2. Experimental reagents.

Foaming Agent	Type	Manufacturer
YF-1	Anionic or non-ionic	Shengli Oil Field
ZK25130	Anionic or non-ionic	Qingtian Zhongke plant Technology Co., Ltd.
ZK12200	Anionic or non-ionic	Qingtian Zhongke plant Technology Co., Ltd.
ZK25100	Anionic or non-ionic	Qingtian Zhongke plant Technology Co., Ltd.
YL-3J	Amphoteric	Dongying He Hui chemical Company
GW-1	Fluorinate	Dongguan City, Guangdong Province Changhe new material Co., Ltd.

2.2. Experimental Facility

A GJ-3S high-speed mixer supplied by Qingdao Haitongda Special Instrument Co., Ltd. (Qingdao, China) was used for the stirring foaming operation. It utilizes a Waring Blender to prepare foam with a controllable speed range of 0–15,000 rpm. The instrument utilized for assessing the temperature and salt resistance of the foam under high-temperature and high-pressure conditions was a high-temperature and high-pressure foam evaluator. The structure of the instrument is illustrated in Figure 1. The instrument was equipped with a reaction kettle featuring a visible window, capable of operating at a temperature of 200 °C and pressure of 25 MPa. The interfacial tension and viscoelastic modulus parameters of the system were measured using a model tracer-H interfacial tensiometer (TECLIS, Lyon, France). It is equipped with a high-temperature and high-pressure reactor, capable of withstanding temperatures of up to 120 °C and pressures of up to 15 MPa. The interfacial tension and viscoelastic modulus of various fluids can be measured using hanging drop and oscillation methods, respectively.

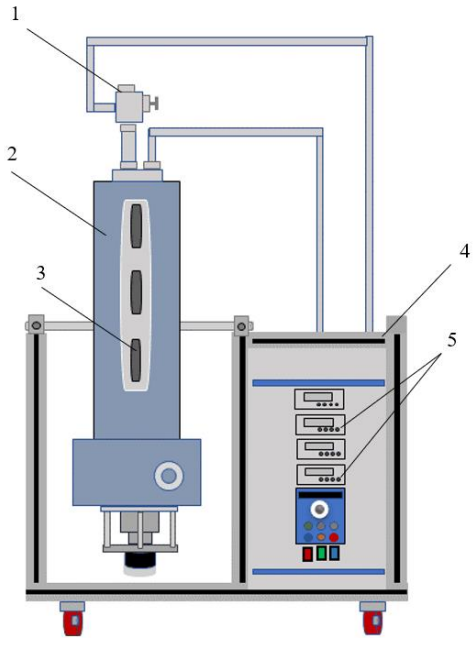


Figure 1. Schematic of the high-temperature and high-pressure foam evaluator. 1, Pressure control valve; 2, electric heating sleeve; 3, visualization window; 4, control box; 5, temperature-pressure digital display.

2.3. Experimental Methods and Procedures

2.3.1. Performance Evaluation of the Foaming Agent

(1) Foaming ability and foam stability measurement: The performance of a foaming agent is evaluated using two key parameters: the initial foaming volume (Vi) and the liquid

drainage half-life ($T_{1/2}$) of the foam it generates. Specifically, Vi quantitatively assesses the foaming ability, while $T_{1/2}$ measures the stability of the foam produced by the agent. The mass concentrations of the surfactants were set at 0.2 wt%, 0.3 wt%, 0.4 wt%, 0.5 wt%, 0.6 wt%, 0.7 wt%, 0.8 wt%, and 0.9 wt%. For each measurement, 100 mL of surfactant solution was poured into a blender. The solution was stirred at 8000 rpm for 3 min and the generated foam was immediately transferred to a glass cylinder to obtain its volume. Then, the foam was kept undisturbed to allow its natural collapse. The time taken for 50 mL of free liquid to drain from the foam was considered the half-life of the foam. A foam with higher stability results in a longer half-life.

(2) Salinity resistance test: In this section, various concentrations of surfactants were dissolved in mineralized water with a salinity of 210,000 mg/L and the foaming volume and half-life of the solutions were measured to evaluate the salt resistance of the foam.

(3) Temperature resistance test: A high-temperature and high-pressure foam evaluator was used for the experiments. The foaming agent was mixed with mineralized water and introduced into the chamber, after which N_2 was injected to ensure that the internal pressure exceeded the saturated vapor pressure at 150 °C. Subsequently, the temperature was increased to 150 °C and the mixture was stirred at 650 rpm for 10 min. The foaming volume and half-life of the foam solution were measured and recorded by an evaluator.

2.3.2. Investigation of Particle-Reinforced Foam Systems

(1) Particle system optimization: Four types of solid particles were selected: fly ash (CF), weathered coal (RC), 1000 mesh graphite (CIK), and graphite milk (LC). These particles, at varying mass fractions, were thoroughly mixed with mineralized water at a concentration of 210,000 mg/L. The mixture was dispersed for 5 min using an ultrasonic dispersion instrument, after which the optimal surfactant was added. The foamability and half-life of the particle-reinforced system were tested. Each experiment was repeated three times and the average value was used as the final result. The solid particles and mass concentrations that exhibited the best performance were selected as standards for subsequent experiments.

(2) Particle size optimization: The foam stabilization effects of 200, 300, and 400 mesh solid particles were evaluated using the Waring–Blender method and the particle size that provided the best foam stabilization performance was optimized.

2.3.3. Measurement of Interfacial Tension and Viscoelastic Modulus Between the Solid Particles and Surfactant

Interfacial tension and viscoelastic modulus measurements were conducted using an interfacial tension meter (Tracker-H, TECLIS Scientific, France) using the hanging drop method. The instrument and equipment were installed and the relevant parameters were inputted into the operation page of the computer. The oscillation period of the experiment was 5 s, the oscillation frequency was 0.2 Hz, and the amplitude was 1 μm^2. Under the driving action of the motor, the solution in the needle dispenses droplets at a specified frequency and volume as determined by the set parameters. The resulting pear-shaped droplet images were captured and transferred to a computer, where specialized software was used to calculate the surface tension using the semi-pairwise method. Finally, the interface expansion viscoelastic modulus was obtained by applying a Fourier transform to the measured data. Each experiment was conducted 3–5 times to ensure the repeatability and reliability of the results. The formula for the interface viscoelastic modulus is presented as Equation (1).

$$E = \frac{d\gamma}{d \ln A} \quad (1)$$

where E-viscoelastic modulus, mN/m; γ-surface tension, and mN/m; A-droplet area, m^2.

3. Results and Discussion

3.1. Evaluation of Conventional Foam Performance Parameters

3.1.1. Optimization of the Foaming Agent Concentration

As illustrated in Figure 2, the foaming volumes of YF-1, ZK25100, YL-3J, and GW-1 initially increased and subsequently stabilized within a concentration range of 0.2% to 0.9%. The foaming volumes of both ZK25130 and ZK12200 remained high within the concentration range of 0.2% to 0.9%, which can likely be attributed to their critical micelle concentrations (CMCs) being below 0.2%. When the mass fraction of ZK25130 was between 0.5% and 0.6%, the foaming volume increased from 385 mL to 440 mL, exhibiting the highest growth rate. The foaming volumes of ZK12200, YF-1, and YL-3J remained at their peak levels when the concentration of the foaming agent was within the range of 0.6–0.8%. Meanwhile, the foaming volumes of ZK25100 and GW-1 were maintained at high levels when the concentration ranges from 0.7% to 0.9%.

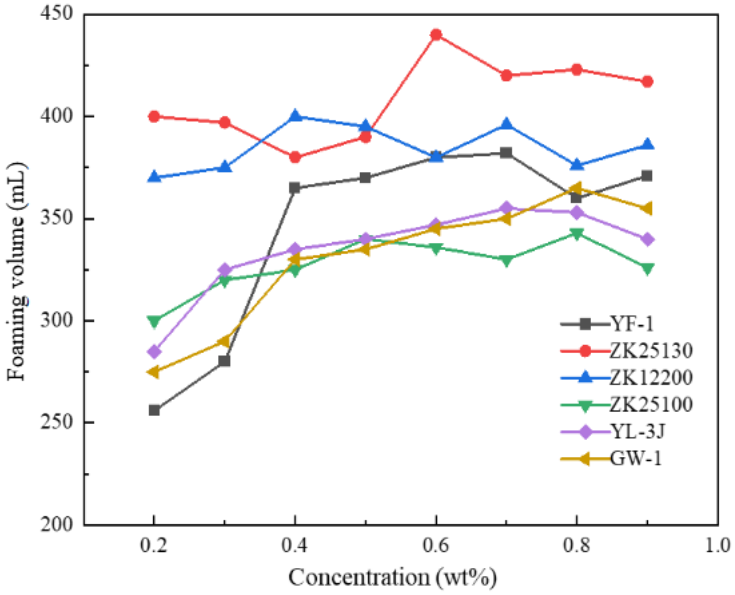


Figure 2. Effects of foaming agent and concentration on foaming volume.

As shown in Figure 3, the half-life initially increased and then stabilized as the concentration of foaming agent increased. Specifically, for YL-3J, the half-life exhibited the most rapid increase when the mass fraction was between 0.3% and 0.4%, followed by a gradual rise before eventually stabilizing, with the maximum half-life reaching 1000 s. This phenomenon can be attributed to the increased surfactant con-centration, which enhances the packing density of the surfactant molecules at the water-air interface, thereby promoting foam formation and stability. The half-lives of ZK25100 and YF-1 reached their maxima at mass fractions of 0.5% and 0.7%, respectively. For ZK25130, the half-life peaked at a mass concentration of 0.3%, after which no significant change was observed. The half-lives of ZK12200 and GW-1 remained relatively stable at varying concentrations of foaming agent.

When the surfactant concentration was in the low range, as the foaming agent concentration increased, the number of surfactant molecules adsorbed on the liquid film surface increased, leading to a gradual increase in surface activity until the maximum adsorption capacity or critical micelle concentration (CMC) was attained [23–26]. With a further increase in the concentration, the stability reaches a plateau. Considering the foaming half-life and foaming volume, the foam composite index (de-fined as the product of foaming volume and half-life) was compared across various concentration conditions. As illustrated in Figure 4, the optimal concentrations for YL-3J, YF-1, and ZK12200 were 0.7%, while those for ZK25100, ZK25130, and GW-1 were 0.5%, 0.3%, and 0.8%, respectively. Based on these

findings, YL-3J exhibited the highest foaming ability at an optimal concentration. However, considering the specific conditions of carbonate fracture-vuggy reservoirs, which involve high temperatures and salinity, further testing is required to evaluate the stability of the foam system under varying temperature and salinity conditions.

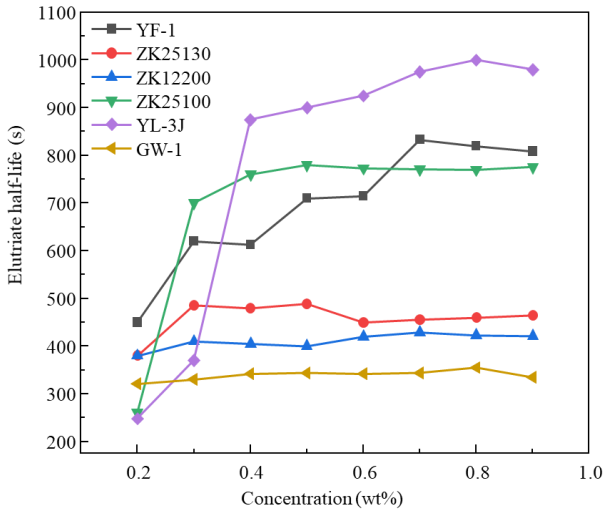


Figure 3. Effect of foaming agent concentration on half-life.

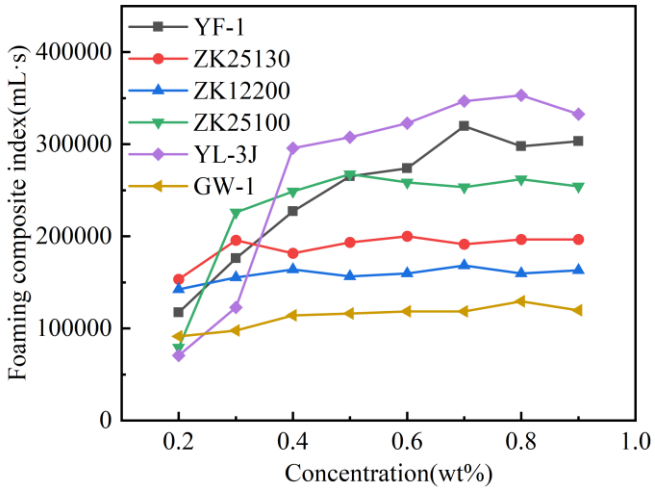


Figure 4. Effects of foaming agent and concentration on foam composite index.

3.1.2. Effect of Salinity on Foam Performance

Because of the flocculation and deposition of YF-1 and ZK12200 surfactants in the formation water environment, they were unsuitable for further study. Consequently, they were excluded and the properties of the remaining four surfactants were studied. Figure 5 shows a comparative analysis of the salt resistance of various surfactants at their optimal concentrations. At a salinity of 210,000 mg/L, 0.3% ZK25130 exhibited a significantly higher foaming performance than the other surfactants, followed by YL-3J. The ZK25120 sample exhibited the lowest foaming performance. However, YL-3J had a higher half-life than the other surfactants, indicating its superior salinity resistance. In addition, the foam formed by YL-3J at high salinity was more uniform, with a denser surface and higher viscosity, demonstrating good sealing characteristics.

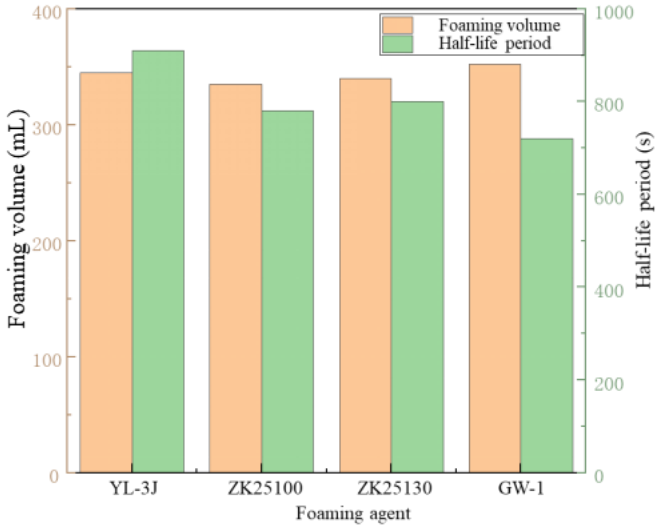


Figure 5. Comparison of the salinity resistance of different foaming agents.

3.1.3. Effect of Temperature on Foam Performance

As illustrated in Figure 6, the foaming agents YL-3J, ZK25100, ZK25130, and GW-1 exhibited significantly higher foam composite indices at 150 °C. The foaming volume increased by more than three times compared with the initial volume, and the half-life of the foam exceeded 10 min. These results indicate that the four foaming agents exhibited good temperature resistance. The half-life of YL-3J at 150 °C was the longest, up to 15 min, whereas that of ZK25130 reached 13 min. Laboratory tests demonstrated that the YL-3J foaming agent exhibited superior temperature and salt resistance, making it suitable for high-temperature and high-salinity conditions. After a comprehensive evaluation, the YL-3J surfactant with a 0.7% mass concentration was selected for subsequent studies.

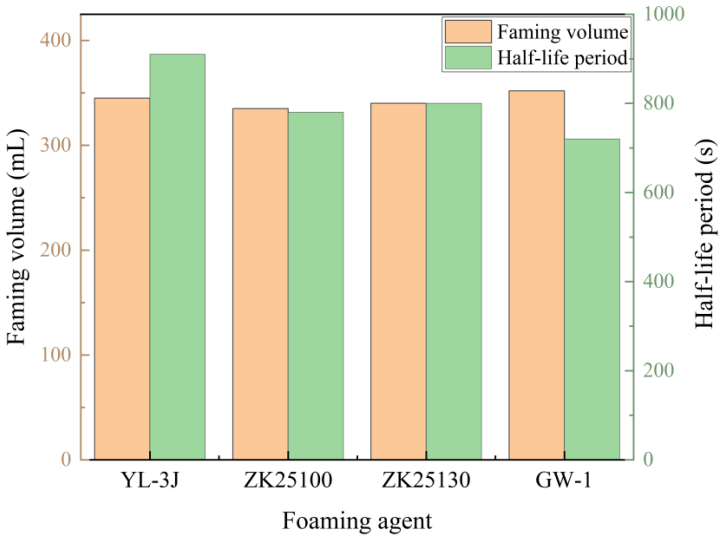


Figure 6. Comparison of temperature resistance of different foaming agents.

3.2. Evaluation of Performance Parameters of the Solid Particle-Reinforced Foam System

3.2.1. Evaluation of the Particle-Reinforced Foam System at Room Temperature

To further enhance foam stability under high-temperature and high-salinity conditions, this study builds on previous research that has optimized the foaming agent concentration. The current approach involves incorporating solid particles into an optimized foam system to improve its robustness and overall performance [27–29]. In this study, solid particle solutions with concentrations ranging from 3% to 21% were prepared and the

foam performance of the foaming agent at the optimal concentration was compared by adding solid particles with different mass concentrations. Figure 7a illustrates the foam performance of foaming agent YL-3J (0.7%) with varying mass concentrations of fly ash. Figure 7b depicts the foam performance of foaming agent YL-3J (0.7%) with different mass concentrations of weathering coal. Figure 7c presents the foam performance of the foaming agent YL-3J (0.7%) with various mass concentrations of 1000 mesh graphite. Figure 7d shows the foam properties of foaming agent YL-3J (0.7%) in graphite milk at different mass concentrations. It can be observed that the addition of solid fly ash particles significantly reduced the foaming volume, decreasing from 375 mL to 335 mL. The half-life initially increased and then stabilized, reaching a maximum of 6420 s (107 min) at a mass concentration of 15%. This represents an increase of 91 min compared to the condition without added particles. Similarly, the addition of weathered coal solid particles reduced the foaming volume and increased its half-life [30–32]. When the mass concentration reached 18%, the half-life extended up to 8160 s, but the foaming volume decreased to only 300 mL. Therefore, the optimal mass concentration of weathered coal is 15%, which increases the half-life by 118 min compared with the condition without added solid particles. The addition of 1000-mesh graphite particles significantly reduced both the foaming volume and half-life of the foaming agent. However, the addition of graphite milk enhanced the foam stability, with a half-life of up to 34 min at a mass concentration of 12%, which is 18 min longer than that of the pure foaming agent.

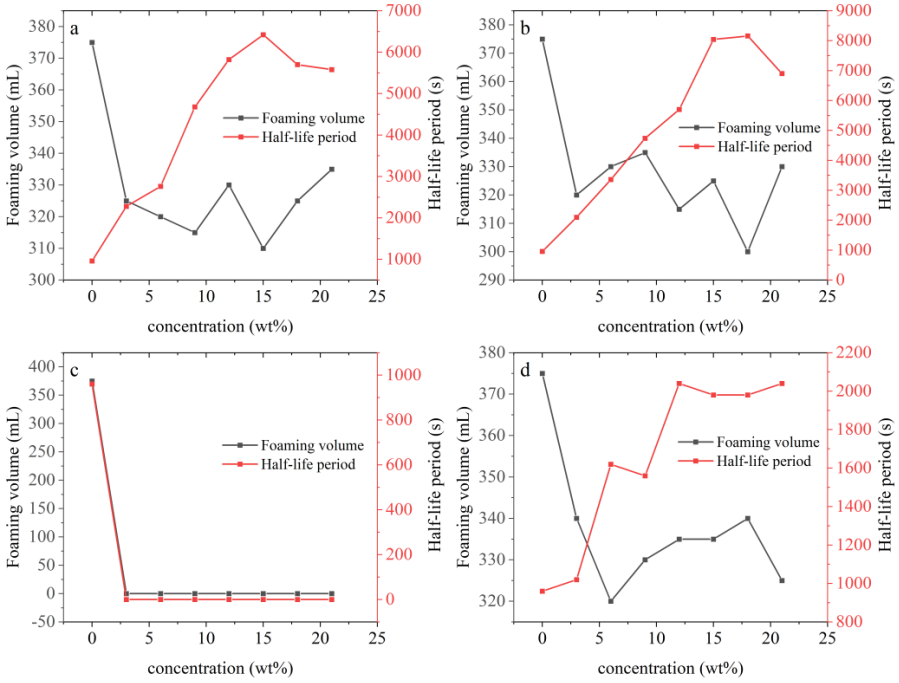


Figure 7. Performance of foam system strengthened by fly ash (**a**), weathering coal (**b**), 1000 mesh graphite (**c**), and graphite milk (**d**) with different mass concentrations.

From the above results, it is evident that both fly ash and weathered coal significantly affected foam stability, with weathered coal having a stronger impact, as shown in Figure 8. As solid particles, weathered coal tends to migrate to the interface of the bubble liquid film, where it forms an adsorption layer skeleton. This reduces the interfacial tension at the liquid film interface, which, in turn, decreases the foaming volume, leading to a reduction in the overall foaming volume of the system when mixed with weathered coal [33]. However, the smaller foam structure resulting from the reduced interfacial tension contributed to the formation of a denser, high-strength foam, which significantly stabilized the skeletal structure of the foam. This slows foam coalescence and reduces the

rate of liquid drainage [34]. Therefore, this study further investigated the use of weathered coal at 5% concentration as solid particles in a strengthened foam system for a more systematic analysis.



(**a**) (**b**)

Figure 8. Comparison of foaming performance of weathered coal and fly ash reinforced foam system. (**a**) Weathered coal reinforced foam system. (**b**) Fly ash reinforced foam system.

Based on previous work, the impact of weathered coal particle size on the performance parameters of the foam was further investigated. The influence of weathered coal with different particle sizes on foam properties is illustrated in Figure 9a–c. It is evident that the foam stabilization effect of solid particles with a 300 mesh size is marginally superior to that of particles with a 400 mesh size and significantly better than that of particles with a 200 mesh size. Particles that are either too large or too small negatively impact foam stabilization. When solid particles are adsorbed onto the liquid film, larger particles tend to detach early because of gravity as liquid drainage progresses, whereas smaller particles exhibit low adsorption free energy. Both factors reduce the foam stability. In contrast, particles of an optimal size are closely packed within the foam's liquid film, forming viscoelastic structures that slow down liquid drainage, thereby enhancing foam stability.

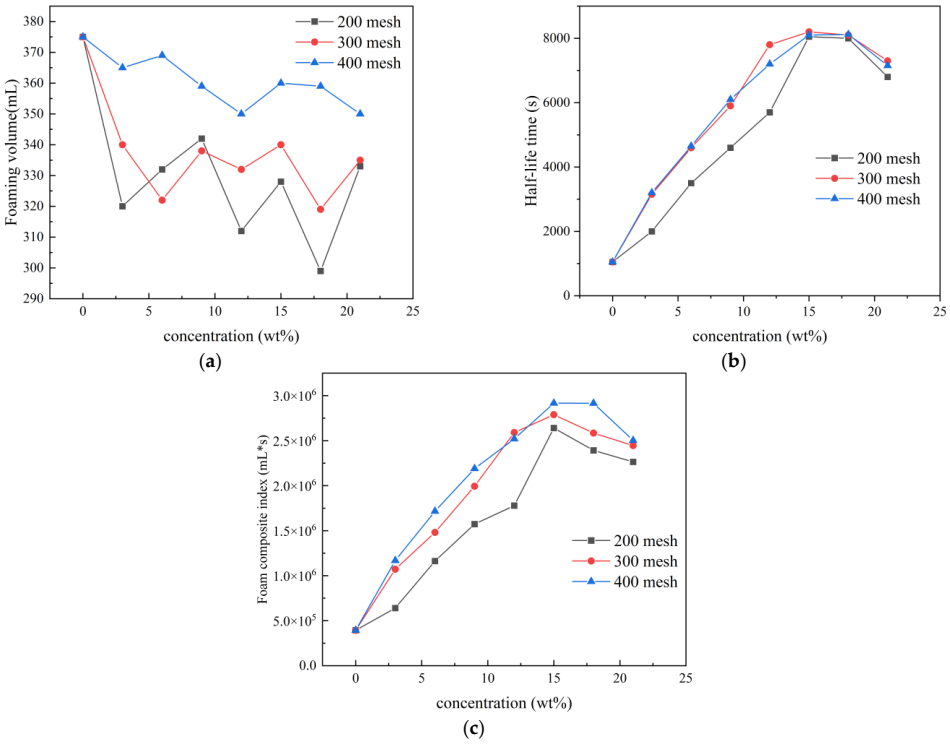


Figure 9. Effect of weathered coal with different particle sizes on the foam properties. (**a**) Effect of weathered coal particles with different mesh numbers on the foam volume. (**b**) Effect of weathered coal particles with different mesh numbers on the half-life. (**c**) Effect of weathered coal particles with different mesh numbers on the foam composite index.

3.2.2. Evaluation of Particle-Reinforced Foam System Under High Temperature and High Salinity

The performances of the particle-reinforced foam system under high-temperature and high-salinity conditions are presented in Table 3. At 150 °C, the foam volume was 310 mL, which was slightly lower than that at normal temperature, and the half-life decreased from 8040 to 1920 s. An increase in temperature reduced the half-life of the foam by 76%, significantly compromising its stability. As a foam stabilizer, weathered coal is dispersed throughout the foam, forming a skeletal structure that effectively delays and mitigates polymerization and disproportionation of the foam [35]. In areas where solid particles accumulate, the increasing viscosity of the liquid film surface hinders the drainage of the liquid film, reducing the frequency of bubble rupture and enhancing the foam stability. The particles at the interface between the bubble and liquid film generated strong capillary forces, causing the aggregated foam to be separated by these forces, which effectively prolonged the half-life of the foam [36,37]. However, when the temperature was too high, the liquid in the film evaporated rapidly, leading to a significant reduction in the thickness of the liquid film. This creates a pressure difference between the liquid film surface and the bulk liquid, which can lead to cracking of the film. In addition, high temperatures accelerate molecular movement, creating a pressure difference between large and small bubbles. Typically, the pressure within smaller bubbles is higher than that within larger bubbles. Consequently, under the influence of this pressure difference, the gas diffused from the smaller bubble to the larger bubble, ultimately resulting in bubble rupture. Overall, the effect of weathered coal particles in optimizing the temperature and salt resistance of the system is evident, as they delay the foam drainage rate and enhance the structural strength of the bubble liquid film.

Table 3. Comparison of the properties of particle-reinforced foam systems.

System	Conditions	Foaming Volume/mL	Half-Life Period/s	Foam Composite Value/mL·s
0.7%YL-3J + 15% Weathered coal	20 °C	325	8040	2,613,000
	150 °C	310	1920	595,200

3.3. Mechanisms of Foam Stabilized by the Surfactant and Solid Particle

3.3.1. Analysis of Foam Stability Mechanism of the Surfactant

Foam is a thermodynamically unstable system with a high surface energy. As a foaming component in the system, the surfactant effectively reduces the interfacial tension of the foam liquid film, thereby enhancing both foaming and foam stability. In addition, the surfactant agent improved the viscoelastic modulus of the system, resulting in a greater pressure gradient change in the foam when the shear was disturbed by reservoir pores. This enhances the foam recovery and shear resistance, providing a foundation for long-term stable flow in the reservoir. Figure 10 shows that the interfacial tension of the surfactant solution in the N_2 environment gradually decreased with increasing surfactant concentration. However, the reduction in surface tension diminishes when the concentration reaches 0.7% wt. The viscoelastic modulus first increased and then decreased, reaching a maximum value at a concentration of 0.7% wt. At low surfactant concentrations, the molecules predominantly exist as monomers or small aggregates, forming a thin film at the gas-liquid interface, which results in a low viscoelastic modulus. As the surfactant concentration increased, the molecules packed more closely, forming micelles or other aggregates. This strengthened the film and increased its elasticity and viscosity. However, at very high concentrations, surfactant molecules saturate the interface, potentially destabilizing the bubble film, increasing the interfacial tension, and reducing the viscoelastic modulus. It

can be observed that the optimal surfactant concentration for YL-3J, resulting in the foam with the best performance, is 0.7%, which is consistent with the previous research findings.

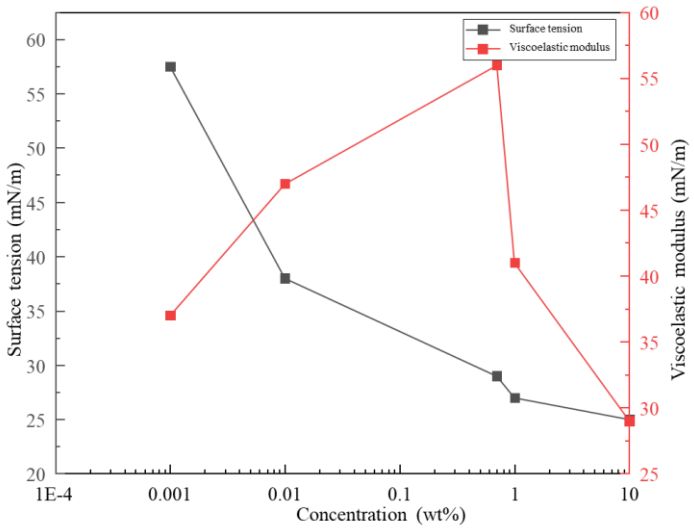


Figure 10. Interface properties of foaming solutions with different concentrations of YL-3J.

3.3.2. Analysis of Foam Stability Mechanism of the Weathered Coal Particle-Reinforced Foam System

Figure 11 shows the surface properties of the reinforced foam system with different concentrations of weathered coal particles. It can be seen that the increase of particle concentration effectively reduces the interfacial tension of surfactant solution in N_2 and enhances the viscoelastic modulus of the system. The weathered coal particles in the formed foam tend to adsorb at the interface of the liquid bubble film, forming a skeleton adsorption layer that can reduce the interfacial tension of the liquid film and improve its mechanical strength. The particle strengthening system generates bubbles with smaller sizes and higher viscoelastic modulus, promoting the formation of a high-strength foam with a dense structure. This effectively reduces the drainage and defoaming rates of the foam system. Building on the surfactants mentioned above, the foam stability and structural strength were further optimized, creating favorable conditions for enhancing their overall stability.

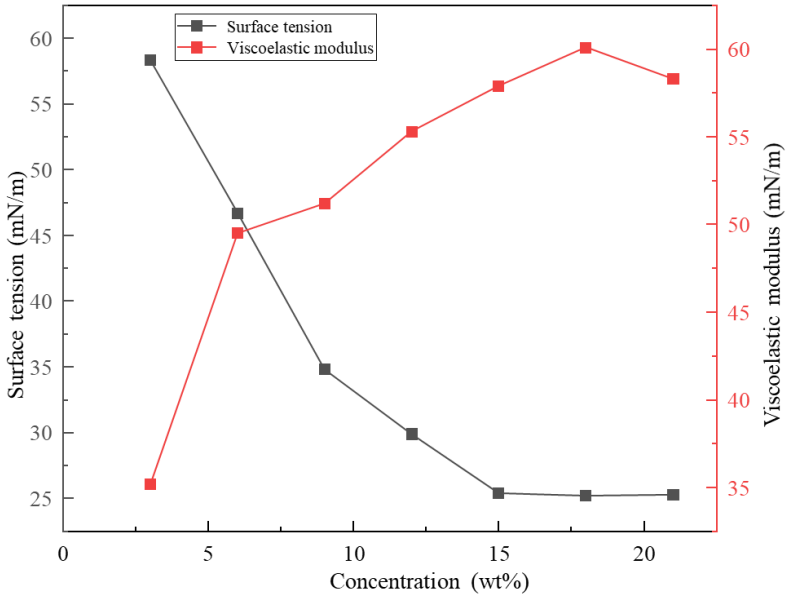


Figure 11. Interface properties of foaming solutions with different solid particle concentrations.

3.3.3. Analysis of the Synergistic Mechanism Between Weathered Coal Particles and Surfactant

Based on previous studies, the mechanism by which the synergistic action of weathered coal particles and surfactants enhances the stability and structural strength of the foam system has been summarized. In a system comprising weathered coal particles mixed with surfactants, the particle surfaces carry negative charges, whereas the amphoteric surfactant YL-3J has both positive and negative charges. This enhancement primarily relies on the attraction between the hydrophobic groups of the surfactant and weathered coal particles. As more YL-3J adsorbed onto the particles, its hydrophobicity weakened. When the hydrophobicity of the particles is weak, most of the particles remain in the liquid phase, and during the foam drainage process, they are transferred to the precipitate along with the liquid phase. However, when a small amount of surfactant is adsorbed onto the particle surfaces, its enhanced hydrophobicity causes most of the particles to remain in the gas phase of the system. In this state, the particles form a relatively stable skeleton structure between the foam liquid film and gas, which slows liquid drainage and improves the water retention rate, as illustrated in Figure 12. Therefore, the adsorption of solid particles onto the liquid film can enhance the mechanical strength of bubbles, delay the drainage of the liquid film, and improve the stability of the system. Surfactants facilitate complete migration and uniform distribution of particles on the liquid film [38].

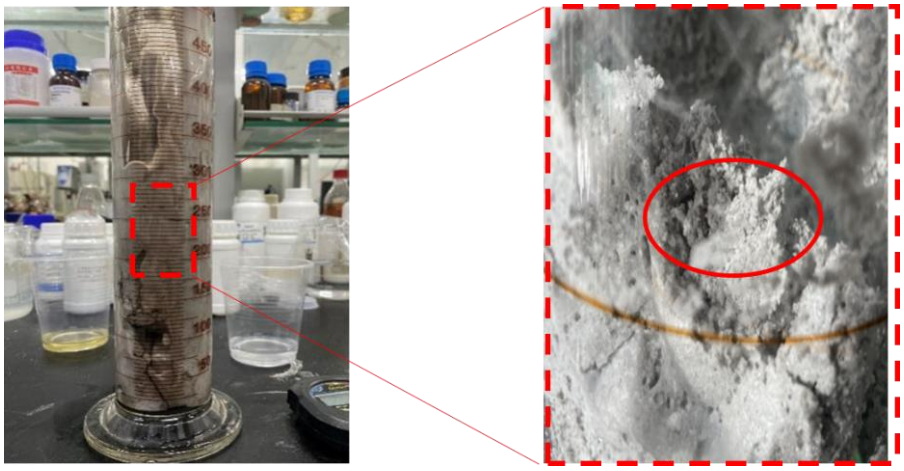


Figure 12. Photograph of weathered coal particle-reinforced foam at room temperature. (Red circle shows that the local amplification of the foam layer).

In addition, because of Laplace pressure, the gas in the foam tends to diffuse from smaller bubbles to larger ones through the liquid film. This resulted in the continuous growth of larger bubbles. As the bubbles increased in size, they eventually merged, leading to foam instability. This process is known as disproportionation, as shown in Figure 13. However, the adsorption of weathered coal particles at the liquid film interface reduces the contact area between N_2 and the liquid film, which can slow the disproportionation caused by N_2 diffusion between the liquid films. Furthermore, the enhancement of the viscoelasticity of the liquid film by surfactants can further assist particles in preventing disproportionation within the system [39].

In addition to the effects mentioned above, both weathered coal and YL-3J can optimize the viscoelastic modulus of the system while significantly reducing the interfacial tension between the liquid phase and N_2. The combination of the two components produces a synergistic effect, with the surfactant-optimized viscoelastic bubble liquid film forming a rigid structure and reduced interfacial tension supported by the particle skeleton. This enhances the foam liquid film's shear resistance and mechanical strength, effectively

slowing the rate of bubble collapse due to liquid drainage and creating favorable conditions for the long-term stable flow of foam in the reservoir. Simultaneously, the dispersion of solid particles and viscoelastic surfactants in the system increased the apparent viscosity of the foam in the reservoir. This positively affects the optimization of the displacement mobility ratio during reservoir development, enhances the sweep efficiency of the system, and further improves oil recovery.

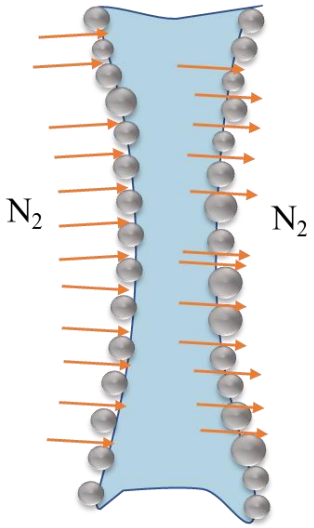


Figure 13. Foam disproportionation diagram.

4. Conclusions

(1) When weathered coal particles were introduced into the foam system, they migrated to the liquid film of the bubbles and formed the skeleton of the adsorption layer. This reduced the interfacial tension of the system, resulting in smaller bubbles and a denser foam structure with enhanced mechanical properties. These changes improved the stability of the foam in high temperature and salinity environments. Additionally, the adsorbed coal particles increased the apparent viscosity and viscoelastic modulus of the system, boosting the resistance of the foam to deformation and reducing the liquid drainage. These effects enhanced the resistance of the foam to temperature and salinity, further contributing to its overall stability.

(2) Large weathered coal particles were easily disturbed by gravity and could not stably remain at the bubble interface, whereas very small particles failed to adsorb onto the liquid film interface because of insufficient adsorption free energy. Consequently, solid particles cannot effectively adsorb at the foam interface, forming a skeleton that enhances the properties of the foam. Therefore, it is crucial to select particles of the optimal size for the foam system to maximize the adsorption effect at the foam interface and improve the subsequent performance.

(3) The weathered coal particles incorporated into the foam system interacted synergistically with the surfactant, whereas the dissolution of ionic surfactants induced electrostatic effects. These effects enhance the adsorption capacity of the particles at the liquid film interface and optimize the structure of the adsorption layer. Additionally, the particles assisted the surfactant in reducing the contact area between the gas phase and the liquid film, thereby mitigating the disproportionation of bubbles. The combined effects significantly improved the mechanical strength and apparent viscosity of the foam, enhancing the system stability and optimizing the displacement mobility ratio during the oil displacement process, ultimately boosting the oil recovery.

Author Contributions: Methodology, Y.X., Y.W. and C.Z.; Formal analysis, L.X. and X.S.; Investigation, Y.X., L.X., Z.K. and B.W.; Data curation, L.X., X.S., Z.K. and B.W.; Writing—original draft, Y.X.; Writing—review & editing, C.Z.; Supervision, C.Z.; Project administration, Y.W. All authors have read and agreed to the published version of the manuscript.

Funding: This research was funded by the National Science and Technology Major Project of China (2016ZX05053) and the Science and Technology Department Project of Sinopec China Petroleum (P11089).

Data Availability Statement: The original contributions presented in this study are included in the article. Further inquiries can be directed to the corresponding author.

Acknowledgments: We are grateful to the Shandong Engineering Research Center for CO_2 Utilization and Storage for their kind help in this study. The valuable comments made by the anonymous reviewers are also sincerely appreciated.

Conflicts of Interest: Authors Yanyan Xu, Linghui Xi, Yajun Wu, Xin Shi, Zhi Kang, Beibei Wu were employed by the company Sinopec Northwest Company of China Petroleum and Chemical Corporation. The remaining authors declare that the research was conducted in the absence of any commercial or financial relationships that could be construed as a potential conflict of interest. The Sinopec Northwest Company of China Petroleum and Chemical Corporation had no role in the design of the study; in the collection, analyses, or interpretation of data; in the writing of the manuscript, or in the decision to publish the results.

References

1. Wang, H.; Lun, Z.; Lv, C.; Lang, D.; Pan, W.; Luo, M.; Wang, R.; Chen, S. Nuclear-magnetic-resonance study on mechanisms of oil mobilization in tight sandstone reservoir exposed to carbon dioxide. *SPE J.* **2018**, *23*, 750–761. [CrossRef]
2. Wang, J.R.; Han, L.; Li, S.Y.; Wang, T. Application status and prospect of foam fluid in oilfield. *Appl. Chem. Ind.* **2012**, *41*, 1408–1411.
3. Liu, L.; Yang, B. Evaluation of enhanced oil recovery by gas injection in low permeability reservoirs. *Chem. Eng. Res. Des.* **2019**, *45*, 62–63.
4. Francols, F.; Chen, W.H.; Chen, W.H.; Gaugiitz, P.A. Experimental and simulation study of high-temperature foam displacement in porous media. *SPE Reserv. Eng.* **1991**, *6*, 37–45.
5. Zhang, C.; Gu, Z.; Cao, L.; Wu, H.; Liu, J.; Li, P.; Zhang, D.; Li, Z. Effect of Pressure and Temperature Variation on Wax Precipitation in the Wellbore of Ultradeep Gas Condensate Reservoirs. *SPE J.* **2023**, *29*, 1589–1604. [CrossRef]
6. Zhang, C.; Liu, Y.; Gu, Z.; Li, P.; Li, Z.; Zhang, K. Chemicals-CO_2 mechanisms of inhibiting steam heat transfer and enhancing oil film strip: Steam flow through the wall-adhering oil film surface in porous medium. *Fuel* **2024**, *356*, 129572. [CrossRef]
7. Pang, Z.X.; Cheng, L.S.; Chen, Y.F. Study on nitrogen foam control technology of water cone in conventional heavy oil bottom water reservoir. *Acta Pet. Sin.* **2007**, *28*, 99–103.
8. Gu, Z.H.; Zhang, C.; Lu, T.; Wang, H.T.; Li, Z.M.; Wang, H.Y. Experimental analysis of the stimulation mechanism of CO_2-assisted steam flooding in ultra-heavy oil reservoirs and its significance in carbon sequestration. *Fuel* **2023**, *345*, 128188. [CrossRef]
9. Fu, J.T.; Zhang, L.; Yin, D.J.; Sui, Z.Q. Plugging and profile control performance of reinforced foam and field test. *Oil Gas Geol. Recovery* **2005**, *12*, 47–49.
10. Wang, M.M.; Guo, D.H. Foaming properties of foams and its influencing factors. *Prog. Fine Petrochem.* **2007**, 40–44+47.
11. Cheng, H. The Enhanced Oil Recovery Effect of Nitrogen-Assisted Gravity Drainage in Karst Reservoirs with Different Genesis: A Case Study of the Tahe Oilfield. *Processes* **2023**, *11*, 2316. [CrossRef]
12. Cheng, H.; Yuan, F.; Zhang, S.; Li, L.; Luo, X.; Chen, B. Investigation on Water Invasion Mode and Remaining Oil Utilization Rules of Fractured-Vuggy Reservoirs: A Case Study of the Intersection Region of S99 Unit in Tahe Oilfield. *Processes* **2023**, *11*, 1833. [CrossRef]
13. Yang, C.H.; Wang, Q.; Dong, J.Y.; Wang, B.; Yang, B.; Chen, Y.H. Research and application of CO_2 flooding foam sealing channeling system in high temperature and high salt reservoir. *Oil Drill. Prod. Technol.* **2012**, *34*, 95–97.
14. Kang, W.L.; Wang, J.; Wu, X.Y.; Xu, B.; Meng, L.W. Study on the stability and influencing factors of amphiphilic polymer foam. *Oilfield Chem.* **2012**, *29*, 48–51, 68.
15. Cheng, H.; Jiang, L.; Li, C. Experimental Study on Production Characteristics of Bottom Water Fractured-Vuggy Reservoir. *Geofluids* **2022**, *2022*, 1–22. [CrossRef]
16. Tang, B.; Ren, K.; Lu, H.; Li, C.; Geng, C.; Wei, L.; Chai, Z.; Wu, S. Study on residual oil distribution law during the depletion production and water flooding stages in the fault-karst carbonate reservoirs. *Processes* **2023**, *11*, 2147. [CrossRef]

17. Tang, B.; Geng, C.; Huang, M.; Lu, H.; Ren, K. Research on the Depletion and Recovery Characteristics of Fault-Karst Reservoirs. *Geofluids* **2022**, *2022*, 1–12. [CrossRef]
18. Liu, P.; Jiang, L.; Tang, B.; Ren, K.; Huang, M.; Geng, C. Residual oil distribution pattern in a fault-solution carbonate reservoir and countermeasures to improve oil development effectiveness. *Geofluids* **2022**, *2022*, 2147200. [CrossRef]
19. Jiang, J.L.; Yue, X.A.; Gao, Z. The role of polymer in the modulation and flooding of foam composite. *Oil Drill. Prod. Technol.* **2011**, *33*, 61–64.
20. Rao, P.; Yang, H.B.; Pu, C.S.; Li, X.H.; Wu, F.P.; Zhang, X.C.; Yang, X.L. Simulation and application of air foam/gel composite flooding technology in shallow ultra-low permeability and low temperature reservoirs. *Appl. Chem. Ind.* **2012**, *41*, 1868–1871.
21. Li, D.; Ren, B.; Zhang, L.; Ezekiel, J.; Ren, S.; Feng, Y. CO_2-sensitive foams for mobility control and channeling blocking in enhanced WAG process. *Chem. Eng. Res. Des.* **2015**, *102*, 234–243. [CrossRef]
22. Li, Z.M.; Wang, P.; Li, S.Y.; Sun, Q.; Li, Y. Progress in improving the stability of carbon dioxide foams with nanoparticles. *J. Southwest Pet. Univ. Nat. Sci. Ed.* **2014**, *36*, 155–161.
23. Sun, Q. *Study on Foam Stabilization Mechanism and Percolation Characteristics of Modified SiO_2 Nanoparticles*; China University of Petroleum: Beijing, China, 2015; Volume 12.
24. Wang, H.; Lun, Z.; Lv, C.; Lang, D.; Luo, M.; Zhao, Q.; Zhao, C. Nuclear-magnetic-resonance study on oil mobilization in shale exposed to CO_2. *SPE J.* **2020**, *25*, 432–439. [CrossRef]
25. Singh, R.; Mohanty, K.K. Synergistic Stabilization of Foams by a Mixture of Nanoparticles and Surfactants. In *SPE Improved Oil Recovery Conference*; SPE 169126-MS; SPE: Richardson, TX, USA, 2014.
26. Espinoza, D.A.; Caldelas, F.M.; Johnston, K.P.; Bryant, S.L.; Huh, C. Nanoparticle-Stabilized Supercritical CO_2 Foams for Potential Mobility Control Applications. In *SPE Improved Oil Recovery Symposium*; SPE-129925-MS; SPE: Richardson, TX, USA, 2010.
27. Binks, B.P.; Fletcher, P.D.; Tian, L. Influence of nanoparticle addition to winsor surfactant microemulsim systems. *Colloids Surf. A Physicochem. Eng. Asp.* **2010**, *363*, 8–15. [CrossRef]
28. Zhang, C.; Li, P.; Lun, Z.; Gu, Z.; Li, Z. Unveiling the Beneficial Effects of N_2 as a CO_2 Impurity on Fluid-Rock Reactions during Carbon Sequestration in Carbonate Reservoir Aquifers: Challenging the Notion of Purer Is Always Better. *Environ. Sci. Technol.* **2024**, *58*, 22980–22991. [CrossRef] [PubMed]
29. Qiu, H.B. Research and application of high temperature three-phase foam profile control agent in Shu 13938 block. *Liaoning Chem. Ind.* **2010**, *39*, 614–617.
30. Wang, S.; Feng, Q.; Javadpour, F.; Hu, Q.; Wu, K. Competitive adsorption of methane and ethane in montmorillonite nanopores of shale at supercritical conditions: A grand canonical Monte Carlo simulation study. *Chem. Eng. J.* **2019**, *355*, 76–90. [CrossRef]
31. Liu, Y.; Rui, Z. A Storage-Driven CO_2 EOR for Net-zero Emission Target. *Engineering* **2022**, *18*, 79–87. [CrossRef]
32. Liu, Y.; Rui, Z.; Yang, T.; Dindoruk, B. Using Propanol as an Additive to CO_2 For IMPRoving CO_2 Utilization and Storage in Oil Reservoirs. *Appl. Energy* **2022**, *311*, 118640. [CrossRef]
33. Zhang, Y.X. Research and application of high temperature three phase foam profile control agent. *Chem. Eng. Equip.* **2013**, *15*, 33–35. [CrossRef]
34. Fujii, S.; Ryan, A.J.; Armes, S.P. Long-range structural order, moiré patterns, and iridescence in latex-stabilized foams. *J. Am. Chem. Soc.* **2006**, *128*, 7882–7886. [CrossRef] [PubMed]
35. Li, X.D.; Fu, M.L.; Hu, J.N. Preparation and Performance Evaluation of Temperature-Resistant and Salt-Resistant Gels. *Gels* **2024**, *10*, 337. [CrossRef] [PubMed]
36. Bai, B.; Liu, Y.; Coste, J.P.; Li, L. Preformed particle gel for conformance control: Transport mechanism through porous media. *SPE Reserv. Eval. Eng.* **2004**, *10*, 89648.
37. Liu, Y.; Ma, X.; Li, H.A.; Hou, J. Competitive Adsorption Behavior of Hydrocarbon(s)/CO_2 Mixtures in a Double-nanopore System using Molecular Simulations. *Fuel* **2019**, *252*, 612–621. [CrossRef]
38. Liu, Y.; Li, H.A.; Okuno, R. Measurements and Modeling of Interfacial Tension of CO_2-CH_4-brine System at Reservoir Conditions. *Ind. Eng. Chem. Res.* **2016**, *55*, 12358–12375. [CrossRef]
39. Liu, Y.; Hou, J. Selective Adsorption of CO_2/CH_4 Mixture on Clay-rich Shale using Molecular Simulations. *J. CO2 Util.* **2020**, *39*, 101143. [CrossRef]

Disclaimer/Publisher's Note: The statements, opinions and data contained in all publications are solely those of the individual author(s) and contributor(s) and not of MDPI and/or the editor(s). MDPI and/or the editor(s) disclaim responsibility for any injury to people or property resulting from any ideas, methods, instructions or products referred to in the content.